Journal of Power Sources 243 (2013) 336–342

Contents lists available at SciVerse ScienceDirect

Journal of Power Sources

journal homepage: www.elsevier.com/locate/jpowsour

Vanadium carbide and graphite promoted Pd electrocatalyst for ethanol oxidation in alkaline media

Zaoxue Yan [a,b,c], Mingmei Zhang [a], Jimin Xie [a,*], Pei Kang Shen [b,c,**]

[a] School of Chemistry and Chemical Engineering, Jiangsu University, Zhenjiang 212013, PR China
[b] State Key Laboratory of Optoelectronic Materials and Technologies, School of Physics and Engineering, Sun Yat-sen University, Guangzhou 510275, PR China
[c] Guangdong Province Key Laboratory of Low-carbon Chemistry & Energy Conservation, School of Physics and Engineering, Sun Yat-sen University, Guangzhou 510275, PR China

HIGHLIGHTS

- V_8C_7 particles (1–3 nm) on graphitized ion-exchange resin are synthesized.
- V_8C_7 and its precursor catalyze the graphitization reaction of resin.
- V_8C_7 promotes the activity of Pd due to synergistic effect.
- Graphite promotes the stability of electrocatalyst due to electrochemical inertia.
- Graphite reduces the overpotential due to high electric conductivity.

GRAPHICAL ABSTRACT

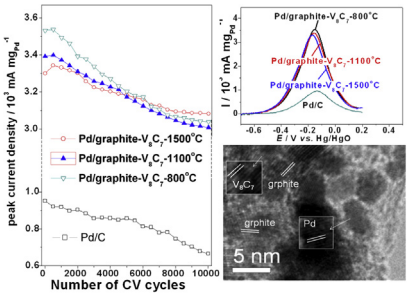

ARTICLE INFO

Article history:
Received 7 April 2013
Received in revised form
7 June 2013
Accepted 10 June 2013
Available online 19 June 2013

Keywords:
Vanadium carbide
Palladium electrocatalyst
Ethanol oxidation
Graphitization
Ion-exchange resin

ABSTRACT

The vanadium carbide particles with the diameter of 1–3 nm on graphitized resin (GC-V_8C_7) are synthesized through ionic exchange process. The materials are characterized by XRD, Raman, TEM, SEM and EDS measurements. The results prove that the ion-exchange resin as both carbon source and dispersion media favors the formation of very uniform and small (1–3 nm) V_8C_7 particles, and protect the V_8C_7 from conglomeration even at the temperature of 1500 °C. Meanwhile, the vanadium compound is found efficient catalytic effect on graphitization of ion-exchange resin, leading to high graphitization degree of GC-V_8C_7. Pd particles are loaded on the GC-V_8C_7 materials as electrocatalyst (Pd/GC-V_8C_7) for ethanol oxidation in alkaline media. The cyclic voltammograms measurements show that both V_8C_7 and GC (graphitized ion-exchange resin) give Pd electrocatalyst improved catalytic performance in activity, stability and overpotential, compared with that of Pd supporting on Vulcan XC-72 carbon (Pd/C). The present synthesizing method of GC-V_8C_7 is simple and effective, which can be readily scaled up for mass production of other nanomaterials.

1. Introduction

Transition metal carbides have been extensively studied as suitable catalyst in chemical synthesis [1], hydrogenation [2], dehydrogenation [3] and isomerization [4] due to the Pt-like property. Typically, the Pt-like catalytic property of tungsten carbide (WC) for chemical catalysis was attributed to a change of

* Corresponding author. Tel.: +86 11 88791708; fax: +86 11 88791800.
** Corresponding author. State Key Laboratory of Optoelectronic Materials and Technologies, School of Physics and Engineering, Sun Yat-sen University, Guangzhou 510275, PR China. Tel.: +86 20 84036736; fax: +86 20 84113369.
E-mail addresses: Xiejm391@sohu.com, earlylearn@163.com (J. Xie), stsspk@mail.sysu.edu.cn (P.K. Shen).

0378-7753/$ – see front matter © 2013 Elsevier B.V. All rights reserved.
http://dx.doi.org/10.1016/j.jpowsour.2013.06.063

electron distribution of the tungsten by the addition of carbon [5]. It was also reported that the addition of WC to Pt, Pd, Au and other noble metals can improve the electrocatalytic activity toward the oxygen reduction reaction (ORR) and alcohol oxidation reaction (AOR) in both acidic and alkaline solutions [6–11]. The improved electrocatalytic activity is believed to be due to the synergistic effect [12–14] between the noble metals and WC. Besides tungsten carbide, molybdenum carbide and vandium carbide were also reported as effective electrocatalyst supports for both ORR and AOR [15–17]. Therein, vandium carbide was reported the most synergistic effect among the three carbides on Pt electrocatalyst for ORR in acidic media [18]. However, it is noted that there was no report concerning the use of vanadium carbide as Pd electrocatalyst support for alcohol oxidation.

There are many methods for preparing vanadium carbide, such as mechanical alloying [19] and thermal decomposition of precursor [20]. These methods lead to large vanadium carbide particles with the sizes from tens to hundreds nanometers. The larger carbide particles have lower surface areas than the commonly used carbon support substrates, resulting in poor dispersion of noble metal nanoparticles. Therefore, the synthesis of vanadium carbide with well-defined particle size is critically important in achieving synergistic effect [11–13,17,21].

Recently, Pd-based electrocatalysts have aroused much attention because they have much higher activity in alkaline media for alcohol oxidation than Pt-based electrocatalysts in both acidic and alkaline media, and also higher than Pd-based electrocatalysts in acidic media [22–26]. More importantly, the alkaline condition is better for fuel cells operation.

Here, we report the preparation of vanadium carbide (V_8C_7) on graphtized ion-exchange resin (GC) with the V_8C_7 particle size of 1–3 nm, Pd nanoparticles were loaded on the support and used for ethanol oxidation in alkaline media. The novelty of this work includes three aspects. Firstly, the ion-exchange resin are used to disperse V_8C_7 precursor and protect the V_8C_7 from conglomeration even at the temperature of 1500 °C. Secondly, V_8C_7 shows the similar synergistic effect as WC on Pd electrocatalyst. Thirdly, V_8C_7 catalyzing graphitization reaction of ion-exchange resin, and consequently improving the stability and reducing the overpotential of the supported electrocatalyst.

2. Experimental

Typically, the D201 × 1 cinnamic strong alkali anion exchange resin (10 g, Hebi power resin factory, China) was impregnated in 100 ml of 0.01 mol L^{-1} NH_4VO_3 solution for 6 h. The exchanged resin was washed with deionized water and dried at 80 °C overnight. The dried resin was then heated at 800 °C (1100 or 1500 °C) for 1 h in N_2 atmosphere. After cooling down to room temperature, the resulting product was grinded into powders to obtain the final vanadium carbide on carbonized resin composite (GC-V_8C_7). The GC-V_8C_7 samples prepared at the temperature of 800, 1100 and 1500 °C were denoted as GC-V_8C_7-800, GC-V_8C_7-1100 and GC-V_8C_7-1500 accordingly. In addition, the resin that was carbonized at 1500 °C for 1 h were used for comparison and denoted as CR-1500.

Pd supported on GC-V_8C_7 (denoted as Pd/GC-V_8C_7), CR-1500 (denoted as Pd/CR-1500) or Vulcan XC-72 carbon (denotes as Pd/C) were prepared and used as electrocatalysts for ethanol oxidation. $PdCl_2$ in 20 ml glycol solution (containing 33.3 mg Pd) was mixed with 50 mg GC-V_8C_7 (CR-1500 or Vulcan XC-72 carbon) and treated in ultrasonic bath for 30 min to form uniform ink. The pH of the mixture was adjusted to 10 by 5 wt% NaOH/glycol solution. The ink was put into a microwave oven (700 W, 2.45 GHz) for intermittent microwave heating at a 20 s on and 20 s off procedure for 10 times. Afterwards, the mixture was washed with water for 4–5 times and dried in vacuum at 80 °C for 2 h. The Pd content in the resulting product was targeted at 40 wt%. The electrocatalysts prepared with GC-V_8C_7-800, GC-V_8C_7-1100 and GC-V_8C_7-1500 were denoted as Pd/GC-V_8C_7-800, Pd/GC-V_8C_7-1100 and Pd/GC-V_8C_7-1500 accordingly.

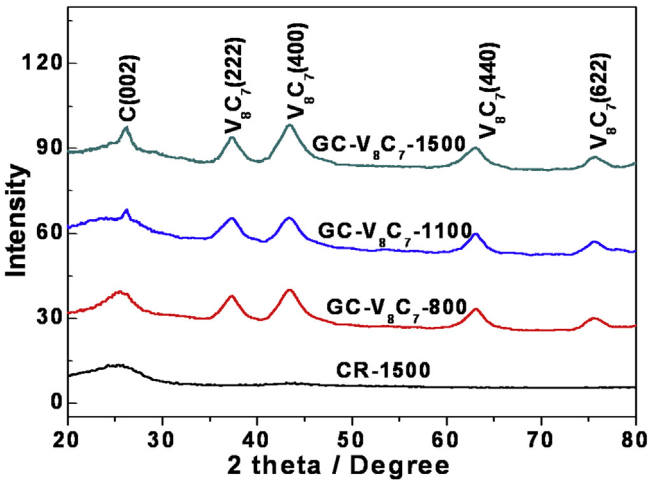

Fig. 1. XRD patterns of GC-V_8C_7-1500, GC-V_8C_7-1100, GC-V_8C_7-800 and CR-1500.

For electrode preparation, Pd/GC-V_8C_7 (Pd/CR-1500 or Pd/C, 5 mg) was dispersed in 1.95 ml ethanol and 0.05 ml 5 wt% Nafion suspension (DuPont, USA) under ultrasonic agitation to form the electrocatalyst ink. The electrocatalyst ink (5 μl) was deposited on a glass carbon electrode and dried at room temperature. The total Pd loadings were 20 μg cm^{-2}. All electrochemical measurements were performed in a three-electrode cell on a potentiastat at 30 °C. A platinum foil (1.0 cm^2) and Hg/HgO were used as counter and reference electrodes, respectively. All chemicals were of analytical grade and used as received.

The morphologies and size of the GC-V_8C_7, CR-1500 and Pd electrocatalysts were characterized by transmission electron microscopy (TEM, JOEP JEM-2010, JEOL Ltd.) operating at 200 kV, and thermal field emission environmental SEM-EDS-EBSD (Quanta 400F, FEI/OXFORD/HKL, Czech/France). The structures were determined on an X-ray diffractometer (XRD, D/Max-IIIA, RigakuCo., Japan,CuK1, $\lambda = 1.54056$ Å radiation). The graphitization degrees of the graphitized carbon were determined by Laser Micro-Raman Spectrometer (Renishaw inVia, Renishaw plc).

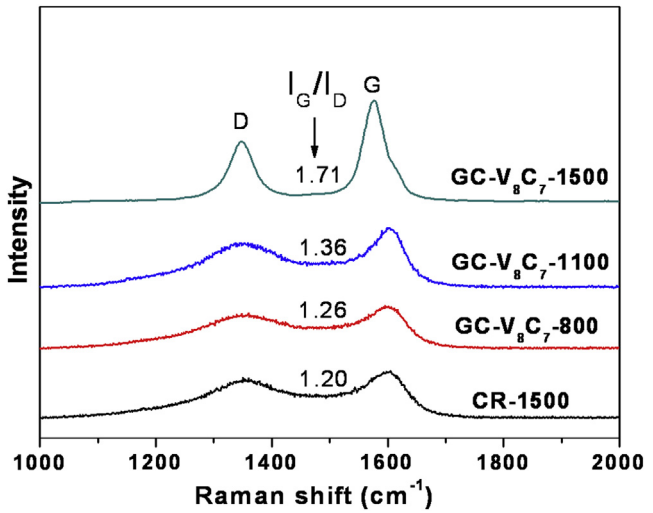

Fig. 2. Raman spectras of the GC-V_8C_7-800, GC-V_8C_7-1100, GC-V_8C_7-1500 and CR-1500.

3. Results and discussion

Fig. 1 shows the XRD patterns of GC-V_8C_7-800, GC-V_8C_7-1100, GC-V_8C_7-1500 and CR-1500. The diffraction peaks at 2θ of 37.4°, 43.4°, 63.0° and 75.6° correspond to (222), (400), (440) and (622) facets of V_8C_7 crystal respectively. The results exhibit that V_8C_7 crystal can be synthesized at 800 °C, and the diffraction peak show hardly any change with the increase of temperature. On the other hand, the diffraction peak at 2θ of 26.4° corresponds to (002) facet of graphite crystal. It shows that GC-V_8C_7-1100 and GC-V_8C_7-1500 (with vanadium compound) have obvious graphite peaks, and the peak intensity increases with the increase of temperature. However, CR-1500 (without vanadium compound) has no obvious graphite peaks even it was heated at 1500 °C. The results indicate that vanadium compound could catalyze the graphitization reaction of the ion exchange resin.

The V_8C_7 crystal size can be calculated according to the Scherrer's equation:

$$D = K\lambda/(B\cos\theta)$$

where D denotes the average crystal diameter in nm, K the Scherrer constant (0.89), λ the wavelength of X-ray ($\lambda = 0.154056$ nm), B the full width at half maximum (FWHM) of the diffraction peak and θ the corresponding Bragg's diffraction angle. The calculated V_8C_7 crystal sizes in GC-V_8C_7-1500, GC-V_8C_7-1100 and GC-V_8C_7-800 are 3.2, 2.9

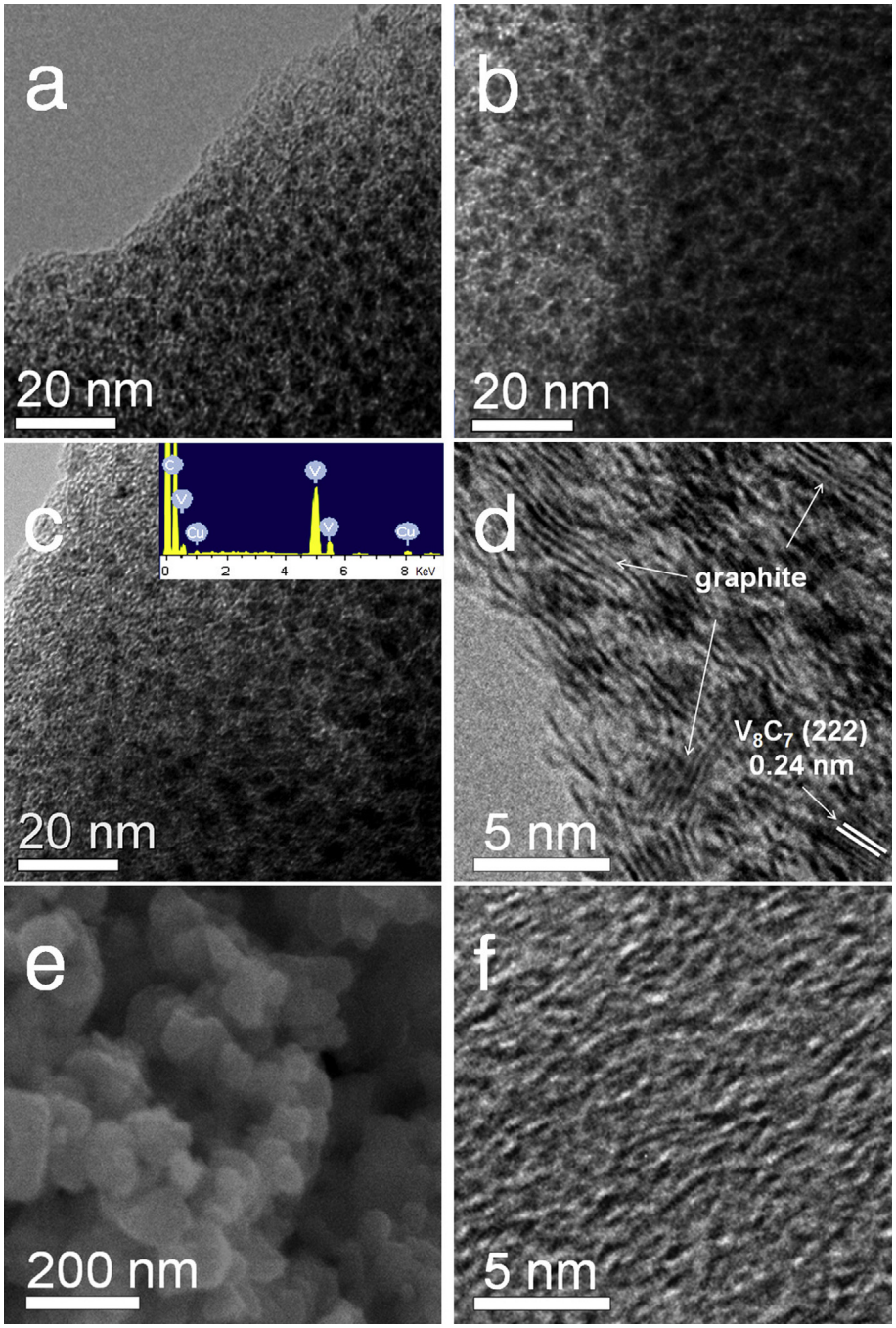

Fig. 3. TEM images of (a) GC-V_8C_7-800, (b) GC-V_8C_7-1100, (c) GC-V_8C_7-1500. (d) HRTEM image of GC-V_8C_7-1500. (e) SEM image of GC-V_8C_7-1500. (f) TEM image of CR-1500. Inset in Fig. 3c is the corresponding EDS pattern.

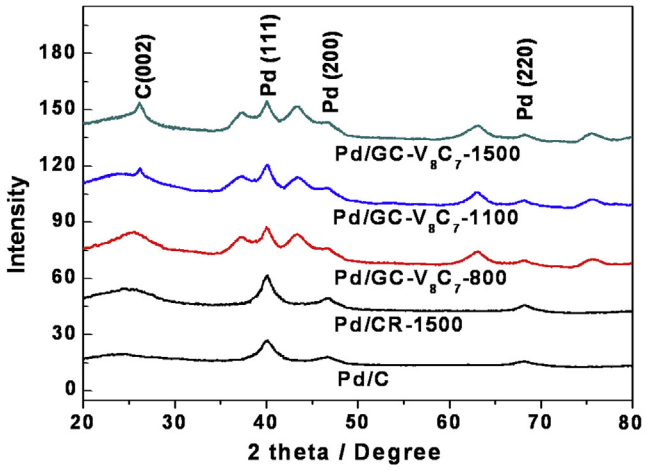

Fig. 4. XRD patterns of Pd/GC-V_8C_7-800, Pd/GC-V_8C_7-1100, Pd/GC-V_8C_7-1500, Pd/CR-1500 and Pd/C.

and 3.0 nm respectively. The results indicate no obvious change of the V_8C_7 crystal size with the temperature variation, which is due to the ion exchange resin being able to disperse the V_8C_7 precursor uniformly and protect the V_8C_7 from conglomeration.

We studied the graphitization degree of the synthesized materials. Fig. 2 shows the Raman spectras of GC-V_8C_7-800, GC-V_8C_7-1100, GC-V_8C_7-1500 and CR-1500. The ratios of the G-band to D-band were used to judge the degree of the graphitization. The G-band at 1584 cm^{-1} corresponds to a splitting of the E_{2g} stretching mode of graphite and reflects the structural intensity of the sp^2-hybridized carbon atom [27]. The D-band at 1350 cm^{-1} is attributed the vibrations of carbon atoms with dangling bonds in disordered graphite planes and the defects incorporated into pentagon and heptagon graphite-like structures. The I_G/I_D values for the above samples were calculated and marked in Fig. 2. In summary, the I_G/I_D values increase with the increase of temperature for the three GC-V_8C_7 samples. However, CR-1500 has the lowest graphitization degree though it was synthesized at the same temperature as GC-V_8C_7-1500. The results confirm the catalytic effect of vanadium compound on graphitization reaction, which is consistent with the XRD results (Fig. 1).

Fig. 3a–c is the TEM images of GC-V_8C_7-800, GC-V_8C_7-1100 and GC-V_8C_7-1500. They all show uniform dispersed V_8C_7 nanoparticles with the diameter about 1–3 nm, confirming no conglomeration occurred even at improved temperature. The EDS pattern in inset of Fig. 3c proves the coexistence of C and V elements. The excrescent peaks of Cu element come from sample bracket. Fig. 3d is the HRTEM image of GC-V_8C_7-1500, which clearly shows the crystal lattices of V_8C_7 (222) and graphite, confirming the coexistence of V_8C_7 and graphite. Fig. 3e is the SEM image of GC-V_8C_7-1500 after ball milling treatment, showing a narrow distribution of particle sizes from 20 to 150 nm. Fig. 3f is the TEM image of CR-1500, which shows no obvious graphite crystal lattices, being consistent with the XRD and Raman results.

It can be imagined that the higher graphitization degree (Figs. 1 and 2) of GC-V_8C_7-1500 have higher electric conductivity and higher corrosion resistance than that of amorphous carbon [28,29].

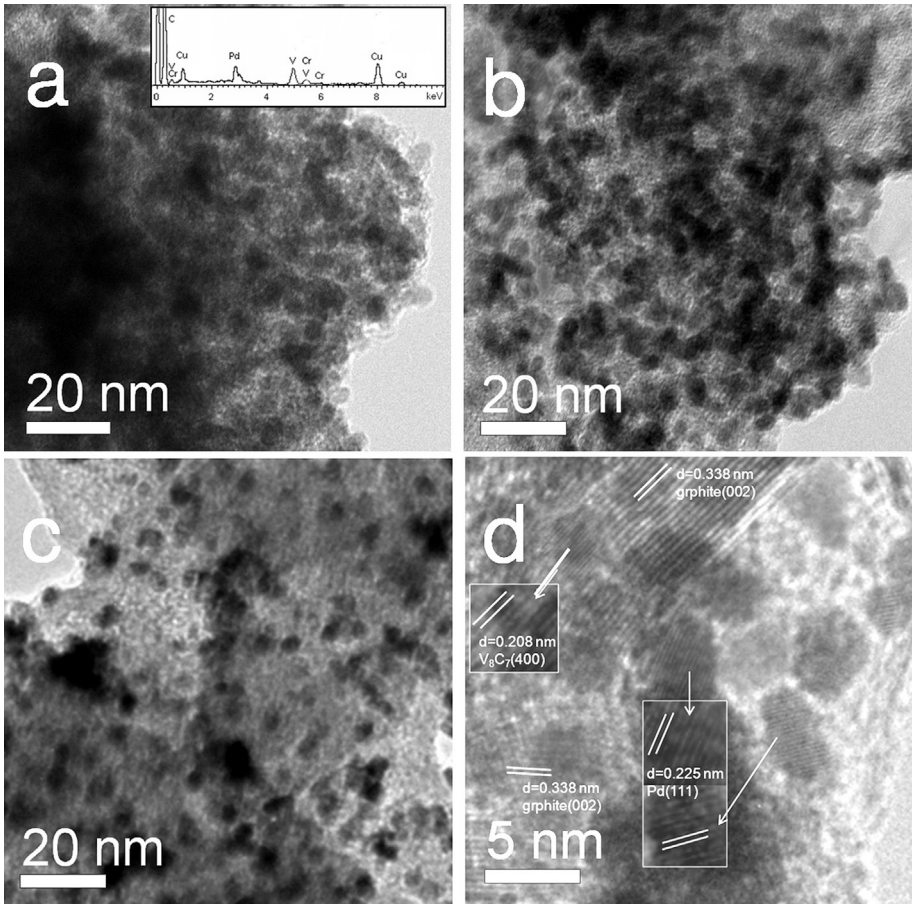

Fig. 5. TEM images of (a) Pd/GC-V_8C_7-1500, (b) Pd/CR-1500 and (c) Pd/C, and (d) the HRTEM image of Pd/GC-V_8C_7-1500. Inset in Fig. 5a is the EDS pattern of Pd/GC-V_8C_7-1500.

Meanwhile, the very small V_8C_7 (Fig. 3c) and GC-V_8C_7-1500 (Fig. 3d) particles could give effective synergistic effect and improved mass transfer properties when used as catalyst support. Pd nanoparticles were therefore loaded on the synthesized GC-V_8C_7 materials and used for ethanol oxidation. Fig. 4 shows the XRD patterns of the synthesized Pd/GC-V_8C_7-800, Pd/GC-V_8C_7-1100, Pd/GC-V_8C_7-1500, Pd/CR-1500 and Pd/C electrocatalysts. The peaks at 2θ of 40.1°, 46.7° and 68.1° correspond to the (111), (200) and (220) facets of Pd crystal. The Pd (220) peak can be used to calculate the Pd crystal size according to the Scherrer's equation mentioned above. And the Pd particle sizes in Pd/GC-V_8C_7-1500, Pd/GC-V_8C_7-1100, Pd/GC-V_8C_7-800, Pd/CR-1500 and Pd/C are accordingly calculated as 5.3 nm, 5.1 nm, 5.0 nm, 5.0 nm and 5.4 nm, respectively. It is obvious that the Pd nanoparticles in all the electrocatalysts have almost the same average diameters.

Fig. 5a–c shows the typical TEM images of Pd/GC-V_8C_7-1500, Pd/CR-1500 and Pd/C electrocatalysts. Most of the Pd nanoparticles in Pd/GC-V_8C_7-1500, Pd/CR-1500 and Pd/C have the diameter range of 4–6 nm, which is consistent with the XRD results (Fig. 4). The inset EDS pattern of Pd/GC-V_8C_7-1500 in Fig. 5a proves the coexistence of Pd, C and V elements. The peaks of Cu and Cr elements come from sample bracket. Fig. 5d is the HRTEM image of Pd/GC-V_8C_7-1500, which clearly shows the V_8C_7 (400), graphite (002) and Pd (111) crystal lattices, further confirming the coexistence of V_8C_7, graphite and Pd.

Fig. 6a compares the cyclic voltammograms of ethanol oxidation on Pd/GC-V_8C_7-800, Pd/GC-V_8C_7-1100, Pd/GC-V_8C_7-1500, Pd/CR-1500 and Pd/C electrocatalysts. The peak current densities and onset potentials for the five electrocatalysts are summarized in Table 1. Among the three Pd/GC-V_8C_7 electrocatalysts, Pd/GC-V_8C_7-800 has the highest peak current density (3535 mA mg_{Pd}^{-1}). Pd/GC-V_8C_7-1100 and Pd/GC-V_8C_7-1500 are slightly inferior to Pd/GC-V_8C_7-800, which might result from their higher graphitization degree. Generally speaking, the higher graphitization degree of supporting materials have more condensed or reduced surfaces, which affect the dispersion of Pd particles and mass transfer, thus reduce the peak current density [28]. However, at the potential under −0.19 V (vs. Hg/HgO), Pd/GC-V_8C_7-1100 and Pd/GC-V_8C_7-1500 have higher current densities than Pd/GC-V_8C_7-800, that is, the formers have more negative onset potentials than the latter. The reason is that the higher graphitization degree of supporting material has higher electric conductivity and lower overpotential [21,28]. Moreover, all the three Pd/GC-V_8C_7 electrocatalysts have more negative onset potentials and higher peak current densities than that of Pd/CR-1500 or Pt/C (Pd/C has the similar peak current density and onset potential with Pd/CR-1500). Typically, the Pd/GC-V_8C_7-1500 (3301 mA mg_{Pd}^{-1}) has 3.61 times higher peak current density and 100 mV more negative onset potential than that of Pd/CR-1500 (951 mA mg_{Pd}^{-1}). It is noticeable that our home-made Pd/C electrocatalyst has fairly well mass activity compares to other Pd/C electrocatalysts reported in literatures [30–34], as shown in Table 2.

Fig. 6b shows the cyclic voltammogram of the five electrodes in 1 mol L^{-1} KOH solution without ethanol. The relative electrochemical surface areas (ECSAs) for the five electrocatalysts can be obtained by calculating the peak areas of the oxidation of Pd. The calculated ECSAs are 1.11, 1.06, 1.03, 0.97 and 1 for Pd/GC-V_8C_7-800, Pd/GC-V_8C_7-1100, Pd/GC-V_8C_7-1500, Pd/CR-1500 and Pd/C respectively (assuming that the ECSA of Pd/C is 1). The results are also summarized in Table 1. Significant things are found by comparing the peak current density and ECSA between the three Pd/GC-V_8C_7 electrocatalysts and Pd/CR-1500 (or Pd/C). Typically, the ECSA ratio of Pd/GC-V_8C_7-1500 to Pd/CR-1500 is 1.14 (see Table 1), however, the ratio of the peak current density of Pd/GC-V_8C_7-1500 to Pd/CR-1500 is 3.61. The increased ratio from 1.14 (ECSA) to 3.61 (peak current density) must result from the promotion effect of V_8C_7 on Pd, since V_8C_7 itself has hardly any catalytic activity on ethanol electro-oxidation (Fig. 6a), which is similar with the synergistic effect between WC and noble metals in literatures [12–14].

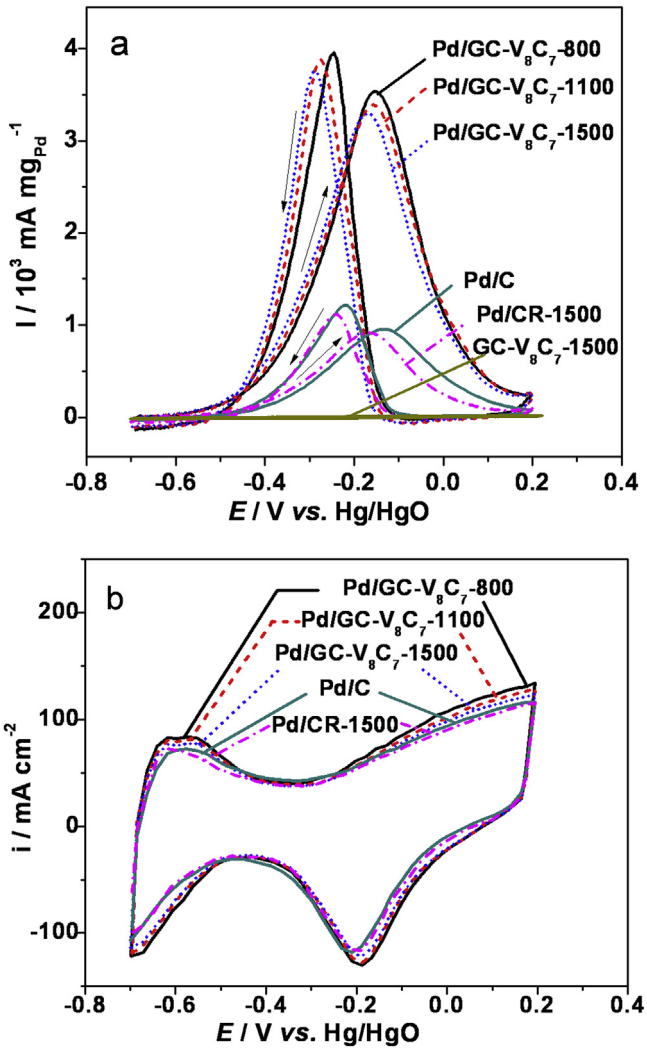

Fig. 6. (a) The cyclic voltammograms of ethanol oxidation on Pd/GC-V_8C_7-800, Pd/GC-V_8C_7-1100, Pd/GC-V_8C_7-1500, Pd/CR-1500, Pd/C and GC-V_8C_7-1500 electrodes in 1.0 mol L^{-1} ethanol/1.0 mol L^{-1} KOH solution with the scan rate of 50 mV s^{-1} at 30 °C, (b) the cyclic voltammograms of the five electrocatalysts in 1.0 mol L^{-1} KOH solution with the scan rate of 50 mV s^{-1} at 30 °C.

The stability of the electrocatalysts on ethanol oxidation is also studied. Fig. 7a shows the relationship between the CV (cyclic voltammogram) cycles and the peak current densities on Pd/GC-V_8C_7-800, Pd/GC-V_8C_7-1100, Pd/GC-V_8C_7-1500 and Pd/C. Fig. 7b is the ratio of peak current densities at different number of CV cycles that are calculated from Fig. 7a. The stability results at the 1st cycle

Table 1
Performances for the five electrocatalysts.

Electrocatalyst	Peak current density/mA mg_{Pd}^{-1}	Onset potential/V	Relative ECSA
Pd/GC-V_8C_7-800	3535	−0.55	1.11
Pd/GC-V_8C_7-1100	3391	−0.55	1.06
Pd/GC-V_8C_7-1500	3301	−0.56	1.03
Pd/CR-1500	915	−0.46	0.97
Pd/C	951	−0.45	1

Table 2
The comparison of the mass activities of various Pd/C electrocatalysts.

Pd/C catalyst	Mass activity (mA mg_{Pd}^{-1})	Experimental conditions
Pd/C (home-made)	951	1 mol L^{-1} KOH + 1 mol L^{-1} ethanol; scan rate 50 mV s^{-1}; 30 °C
Pd/C [30]	879	1 mol L^{-1} KOH + 1 mol L^{-1} ethanol; scan rate 50 mV s^{-1}; 30 °C
Pd/C [31]	85	1 mol L^{-1} KOH + 1 mol L^{-1} ethanol; scan rate 50 mV s^{-1}; 30 °C
Pd/C [32]	314	0.1 mol L^{-1} KOH + 0.5 mol L^{-1} ethanol; scan rate 50 mV s^{-1}; room temperature
Pd/C [33]	628	1 mol L^{-1} KOH + 1 mol L^{-1} ethanol; scan rate 50 mV s^{-1}; room temperature
Pd/C [34]	750	1 mol L^{-1} KOH + 1 mol L^{-1} ethanol; scan rate 50 mV s^{-1}; 30 °C

Table 3
The stability of electrocatalysts.

Electrocatalyst	CV cycle	Peak current density (mA mg_{Pd}^{-1})	Reduced activity
Pd/GC-V_8C_7-800	1st	3535	14.1%
	10,000th	3038	
Pd/GC-V_8C_7-1100	1st	3391	11.2%
	10,000th	3010	
Pd/GC-V_8C_7-1500	1st	3301	6.6%
	10,000th	3082	
Pd/C	1st	951	30.1%
	10,000th	665	

and the 10,000th cycle are summarized in Table 3. It can be seen that the catalytic activities for all the electrocatalyst obviously decreased after 10,000 CV cycles. But the three Pd/GC-V_8C_7 electrocatalysts have more stability than that of Pd/C. Meanwhile, the three Pd/GC-V_8C_7 electrocatalysts including Pd/GC-V_8C_7-800, Pd/GC-V_8C_7-1100 and Pd/GC-V_8C_7-1500 display different stabilities, which might relate to the graphitization degree of GC-V_8C_7 materials. Typically, the GC-V_8C_7-1500 has the highest graphitization degree (Fig. 2) and the Pd/GC-V_8C_7-1500 has the highest stability (Fig. 7). Similarly, the GC-V_8C_7-800 has the lowest graphitization degree (Fig. 2) and the Pd/GC-V_8C_7-800 has the lowest stability (Fig. 7). The results indicate that higher graphitization degree result in higher stability. The reason may be that the graphite has higher chemical and electrochemical inertia, which protect the GC-V_8C_7 from being corroded [21,28]. As a result of the higher stability, Pd/GC-V_8C_7-1500 shows the highest peak current densities after the 6000th cycle (Fig. 7a), showing great advantage as candidate of fuel cell electrocatalyst.

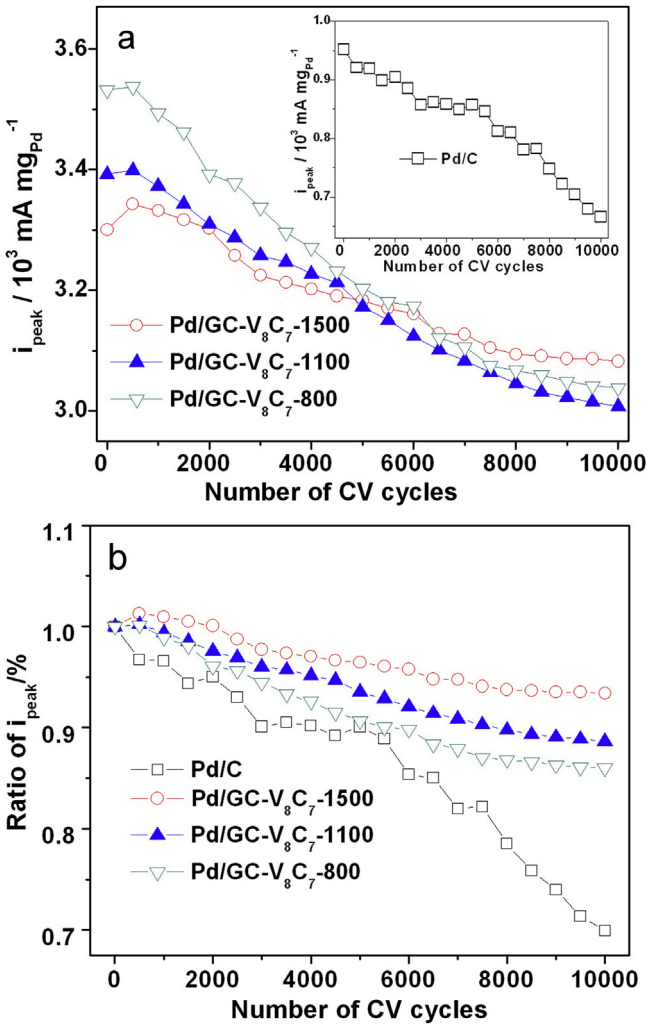

Fig. 7. (a) Relationship between CV (cyclic voltammograms) cycles and peak current density and (b) ratio of peak current density at different number of CV cycles on Pd/GC-V_8C_7-800, Pd/GC-V_8C_7-1100, Pd/GC-V_8C_7-1500 and Pd/C.

In this paper, the V_8C_7 contents in all the GC-V_8C_7 samples are the same, the GC: V_8C_7 ratio increases with the increase of temperature for higher temperature favoring the formation of GC. Therefore, the relation between GC: V_8C_7 ratio and catalytic performance should be the same as the relation between graphitization degree and catalytic performance: On one hand, higher GC: V_8C_7 ratio resulted in lower catalytic activity due to more condensed surfaces and poorer dispersion of Pd particles; on the other hand, higher GC: V_8C_7 ratio led to higher catalytic stability and more negative onset potential due to higher corrosion resistance and higher electric conductivity of graphite (see Figs. 6 and 7).

The mechanism of ethanol oxidation on a palladium electrode in alkaline media had been studied by our previous work [35], in which the electrode performance has been found to depend on the pH of the electrolyte. The best performance was observed in 1 mol L^{-1} NaOH solution (pH = 14), while the electrochemical activity decreased by either increasing or decreasing the NaOH concentration. In situ FTIR spectroscopic measurements showed that the main oxidation product was sodium acetate at NaOH concentrations higher than 0.5 mol L^{-1}. The C–C bond cleavage of ethanol occurred at pH values $\leq$13. However, the catalytic activity for ethanol oxidation was quite low in these conditions. In addition, no CO formation was detected along the oxidation of ethanol by FTIR spectroscopy. As to detecting mechanism of ethanol oxidation on V_8C_7 modified Pd electrocatalyst, more efforts will be needed.

4. Conclusions

The V_8C_7 particles on graphitized resin (GC-V_8C_7) were successfully synthesized through ionic exchange process. The uniform sizes (1–3 nm) of the V_8C_7 particles can be easily obtained by adopting the ion-exchange resin as both carbon source and dispersion agent. The V_8C_7 and its precursor obviously favor the graphitization reaction of the ion-exchange resin. Both V_8C_7 and the graphite gave Pd-based electrocatalyst improved catalytic performance for ethanol oxidation in alkaline media. Therein, V_8C_7 improved the peak current density and reduced the onset potential, which is similar with the synergistic effect between WC and Pt [12–14]; the graphite improved the stability and further reduced the onset potential, which is due to the electrochemical inertia and

higher electric conductivity of graphite [28]. The multi-effects of V_8C_7 and graphite on Pd make Pd/GC-V_8C_7 a highly active and stable fuel cell electrocatalyst candidate.

Acknowledgments

Zaoxue Yan thanks the China Postdoctoral Science Foundation (2012M521011) and College Natural Science Research Program of Jiangsu Province (12KJB150007). Jimin Xie thanks the Science and Technology Support Program of Jiangsu (BE2010144), Natural Science Foundation of Jiangsu (BK2010166) and Social Development Program of Zhenjiang (SH2010025).

References

[1] H. Shou, R.J. Davis, J. Catal. 282 (2011) 83–93.
[2] N. Perret, X. Wang, L. Delannoy, C. Potvin, C. Louis, M.A. Keane, J. Catal. 286 (2012) 172–183.
[3] D.W. Flaherty, S.P. Berglund, C.B. Mullins, J. Catal. 269 (2010) 33–43.
[4] A.-F. Lamic, C.-H. Shin, G. Djéga-Mariadassou, C. Potvin, Appl. Catal. A: Gen. 302 (2006) 5–13.
[5] R.B. Levy, M. Boudart, Science 181 (1973) 547–549.
[6] M. Yin, Q. Li, J.O. Jensen, Y. Huang, L.N. Cleemann, N.J. Bjerrum, W. Xin, J. Power Sources 219 (2012) 106–111.
[7] C.K. Poh, S.H. Lim, Z. Tian, L. Lai, Y.P. Feng, Z. Shen, J. Lin, Nano Energy 2 (2013) 28–39.
[8] X.-B. Gong, S.-J. You, X.-H. Wang, Y. Gan, R.-N. Zhang, N.-Q. Ren, J. Power Sources 225 (2013) 330–337.
[9] M. Nie, P.K. Shen, Z. Wei, J. Power Sources 167 (2007) 69–73.
[10] L. Kuai, X. Yu, S. Wang, Y. Sang, B. Geng, Langmuir 28 (2012) 7168–7173.
[11] R. Wang, C. Tian, L. Wang, B. Wang, H. Zhang, H. Fu, Chem. Commun. 0 (2009) 3104–3106.
[12] G.F. Cui, P.K. Shen, H. Meng, J. Zhao, G. Wu, J. Power Sources 196 (2011) 6125–6130.
[13] Z. Zhao, X. Fang, Y. Li, Y. Wang, P.K. Shen, F. Xie, X. Zhang, Electrochem. Commun. 11 (2008) 290–293.
[14] R. Wang, Y. Xie, K. Shi, J. Wang, C. Tian, P. Shen, H. Fu, Chem. Eur. J. 18 (2012) 7443–7451.
[15] Z. Yan, H. Wang, M. Zhang, Z. Jiang, T. Jiang, J. Xie, Electrochim. Acta 95 (2013) 218–224.
[16] G. He, Z. Yan, M. Cai, P.K. Shen, M.-R. Gao, H.-B. Yao, S.-H. Yu, Chem. Eur. J. 18 (2012) 8490–8497.
[17] Z. Yan, M. Cai, P.K. Shen, J. Mater. Chem. 21 (2011) 19166–19170.
[18] G. He, Z. Yan, X. Ma, H. Meng, P.K. Shen, C. Wang, Nanoscale 3 (2011) 3578–3582.
[19] B. Zhang, Z.Q. Li, J. Alloys Compd. 392 (2005) 183–186.
[20] Z.W. Zhao, H.S. Zuo, Y. Liu, W.Q. Song, S.F. Mao, Y.R. Wang, Int. J. Refract. Met. Hard Mater. 27 (2009) 971–975.
[21] Z. Yan, H. Meng, P.K. Shen, R. Wang, L. Wang, K. Shi, H. Fu, J. Mater. Chem. 22 (2012) 5072–5079.
[22] C. Xu, L. Cheng, P. Shen, Electrochem. Commun. 9 (2007) 997–1001.
[23] K.-H. Ye, S.-A. Zhou, X.-C. Zhu, C.-W. Xu, P.K. Shen, Electrochim. Acta 90 (2013) 108–111.
[24] H. Zhao, J. Yang, L. Wang, C. Tian, B. Jiang, H. Fu, Chem. Commun. 47 (2011) 2014–2016.
[25] N. Tian, Z.-Y. Zhou, N.-F. Yu, L.-Y. Wang, S.-G. Sun, J. Am. Chem. Soc. 132 (2010) 7580–7581.
[26] K. Ding, G. Yang, S. Wei, P. Mavinakuli, Z. Guo, Ind. Eng. Chem. Res. 49 (2010) 11415–11420.
[27] M.S. Dresselhaus, G. Dresselhaus, R. Saito, A. Jorio, Phys. Rep. 409 (2005) 47–99.
[28] Z. Yan, M. Cai, P.K. Shen, J. Mater. Chem. 22 (2012) 2133–2139.
[29] L. Wang, C. Tian, B. Wang, R. Wang, W. Zhou, H. Fu, Chem. Commun. (2008) 5411–5413.
[30] S.T. Nguyen, H.M. Law, H.T. Nguyen, N. Kristian, S. Wang, S.H. Chan, X. Wang, Appl. Catal. B Environ. 91 (2009) 507–515.
[31] F. Hu, X. Cui, W. Chen, J. Phys. Chem. C 114 (2010) 20284–20289.
[32] Y. Suo, I.-M. Hsing, J. Power Sources 196 (2011) 7945–7950.
[33] S.Y. Shen, T.S. Zhao, J.B. Xu, Y.S. Li, J. Power Sources 195 (2010) 1001–1006.
[34] Z. Yan, Z. Hu, C. Chen, H. Meng, P.K. Shen, H. Ji, Y. Meng, J. Power Sources 195 (2010) 7146–7151.
[35] X. Fang, L. Wang, P.K. Shen, G. Cui, C. Bianchinic, J. Power Sources 195 (2010) 1375–1378.